



Carbazole-triazine based donor-acceptor porous organic frameworks for efficient visible-light photocatalytic aerobic oxidation reactions

Journal:	<i>Journal of Materials Chemistry A</i>
Manuscript ID	TA-ART-06-2018-005329.R2
Article Type:	Paper
Date Submitted by the Author:	07-Jul-2018
Complete List of Authors:	Luo, Jian; University of Nebraska-Lincoln, Chemistry Lu, Jingzhi; University of Nebraska-Lincoln, Department of Chemistry Zhang, Jian; University of Nebraska-Lincoln,



Journal Name

ARTICLE

Carbazole-triazine based donor-acceptor porous organic frameworks for efficient visible-light photocatalytic aerobic oxidation reactions

Jian Luo,[†] Jingzhi Lu⁺ and Jian Zhang^{*}Received 00th January 20xx,
Accepted 00th January 20xx

DOI: 10.1039/x0xx00000x

www.rsc.org/

We report the synthesis of a series of carbazole-triazine based donor-acceptor (D-A) POFs and their photocatalytic activities for aerobic oxidation reactions. The simultaneous introduction of carbazole-based electron donor and triazine-based electron acceptor in D-A POFs stabilizes the charge transfer state and enables an efficient triplet-triplet energy transfer to generate ¹O₂. Meanwhile, systematic variation of the D-A distance results in the tunable photoredox properties and consequently the efficiency for generation of reactive oxygen species (ROSs). Upon visible light excitation, all three D-A POFs exhibit excellent capability to promote three aerobic oxidations: sulfides oxidation, oxidative amine coupling, and Mannich reaction. This systematic study validates the design principle of D-A POFs as high-performance photo-oxidation catalysts with wide substrate scope and excellent stability and recyclability.

Introduction

Oxidation is one of the most important chemical transformations, which contributes about 30% of the total output of chemical industry.¹ Many key chemicals and intermediates such as alcohols, aldehydes, ketones, acids, and epoxides are produced from the oxidation process. Oxidation is also an important methodology for the synthesis of drug leading compounds in pharmaceutical chemistry and building blocks in material chemistry.² However, the traditional methods of oxidizing organic compounds require stoichiometric quantities of oxidants that are either highly explosive (e.g. peroxide, H₂O₂, or ClO⁻) or contain toxic heavy metals (e.g. MnO₂ or CrO₄³⁻) and generate large amounts of inorganic salts as by-product.¹ Thus, aerobic oxidation that uses molecular oxygen (O₂) as the green oxidant is an ideal strategy to increase atom economy and address environmental concerns.³ The drawbacks of thermal aerobic oxidation reactions, however, are that they usually rely on catalysts containing transition metals such as Pd, Au, Ru, Ir, and Cu, and oftentimes are carried out at high temperature or under high pressure.⁴

Recently, photocatalytic organic synthesis has received increasing attention due to its mild reaction conditions (near room temperature and atmospheric pressure), simple setup, and environmental benignness.⁵ Transition-metal complexes such as [Ru(bpy)₃]²⁺ (bpy = 2,2'-bipyridine) and *fac*-Ir(ppy)₃ (ppy = 2-phenyl-pyridine) and organic dyes have been widely applied as photocatalysts for organic synthesis,⁶ including aerobic

oxidation reactions.⁷ Meanwhile, metal-free solid materials, such as graphitic carbon nitride (*g*-C₃N₄),⁸ porous organic polymers (POPs),⁹ and π -conjugated porous organic frameworks (POFs and CMPs)¹⁰ have also been developed as heterogeneous visible light photocatalysts. POFs, in particular, with large surface area and permanent nano/mesozized pores, outstanding thermal stability, and highly tunable optoelectronic properties,¹¹ represents an ideal platform for photocatalytic organic transformations. Moreover, due to its highly crosslinked network and particulate nature, POFs can be easily separated and reused.¹² In the past several years, POFs have been used as effective visible light photocatalysts for net oxidative,¹³ net reductive,¹⁴ and redox neutral reactions.¹⁵ In particular, aerobic oxidation of sulfides, amines, alcohols, and arylboronic acids have been realized by using POFs as the photocatalysts.^{13, 16}

It is known that the photocatalytic activity of POFs can be easily adjusted by tuning the photoredox potential (or band gap).¹⁷ Recently, we have developed a statistical copolymerization approach to fine-tune the redox potentials of donor-acceptor (D-A) POFs.¹⁸ However, the random nature of copolymerization could cause a heterogeneity and prevent a better understanding of the structure-activity relationship of the photocatalyst. Herein, we report the photocatalytic activities of D-A POFs that are synthesized via homo-coupling of carbazole-triazine based D-A monomers. This synthetic strategy enables a better control of the distance and ratio between donor and acceptor, and consequently the optoelectronic properties of the resulting D-A polymers. Three POFs with tunable D-A distance, namely, poly-(2,4,6-tri(9*H*-carbazol-9-yl)-1,3,5-triazine) (pTCT), poly-(2,4,6-tris(4-(9*H*-carbazol-9-yl)phenyl)-1,3,5-triazine) (pTCT-P), poly-(2,4,6-tris(4'-(9*H*-carbazol-9-yl)-[1,1'-diphenyl]-4-yl)-1,3,5-triazine) (pTCT-2P), were synthesized (Fig. 1). These D-A POFs upon visible light

Department of Chemistry, University of Nebraska-Lincoln, Lincoln, Nebraska, 68588, United States *E-mail: jzhang3@unl.edu

[†] These authors contributed equally.

Electronic Supplementary Information (ESI) available. See DOI: 10.1039/x0xx00000x

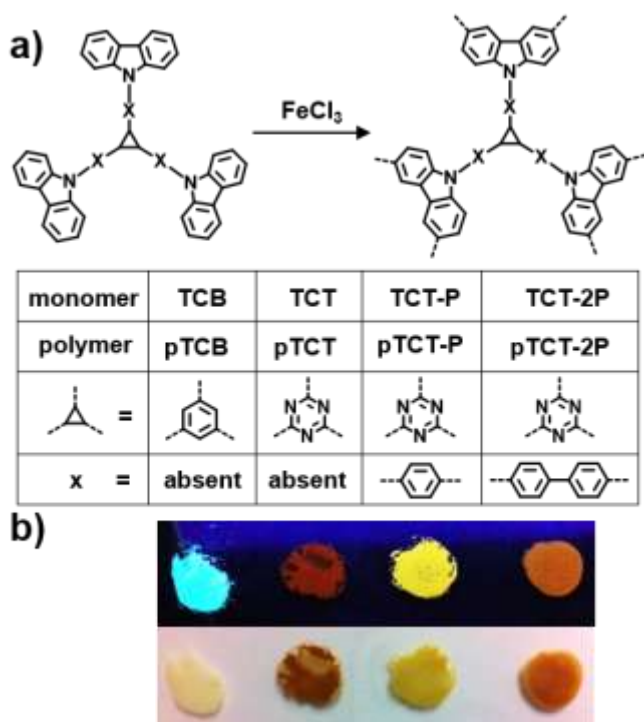


Fig. 1 (a) Chemical structure, synthesis and (b) digital photographs of POFs under UV (365 nm) and visible light.

excitation efficiently generate reactive oxygen species (ROs) and promote prototypic aerobic oxidation reactions such as sulfides oxidation, oxidative amine coupling, and Mannich reaction.

Results and discussion

Synthesis and characterization

The triazine moiety in POFs (e.g. covalent triazine frameworks) is typically formed *in situ* during the polymerization reaction, namely, the trimerization of aromatic nitriles with strong acid (e.g. ZnCl_2 or TfOH) at high temperature.¹⁹ In our work, however, the triazine moiety is prepared before POF synthesis. Specifically, D-A monomers that consist of carbazole and triazine (Fig. 1) were first synthesized through either nucleophilic substitution of 9H-carbazole to 2,4,6-trichloro-1,3,5-triazine (for TCT) or copper catalyzed Ullmann coupling between 9H-carbazole and aryl bromide and aryl iodide (for TCT-P and TCT-2P, respectively) (see ESI S-1 for

details).²⁰ The D-A POFs were prepared using an oxidative polymerization under reflux of a suspension of D-A monomers and FeCl_3 in dry CHCl_3 for 3 days.²¹ Another POF that is only composed of electron donor carbazole, poly-(1,3,5-tri(9H-carbazol-9-yl)benzene (pTCB),²² was also synthesized as a comparison (Fig. 1). During the polymerization process, the carbazole group is oxidized and afford the carbon-centered radical, which further couples to each other to form the crosslinked porous frameworks. The unreacted monomer and iron salt were removed by organic solvent and acidic aqueous solution, and the resulting solid was further purified by Soxhlet extraction. After drying under vacuum, the POFs were obtained as fine powders as shown in Fig. 1b with excellent yields (> 95%). To compare the photocatalytic activities of the POFs and their corresponding monomers, *tert*-butyl group was induced into the 1,3,5-triazine-based monomers to obtain soluble tBuTCT, tBuTCT-P and tBuTCT-2P (see ESI S-1 for details). Note that, the synthesis of pTCT has been previously documented with no description of its photocatalytic properties.²³ Both pTCT-P and pTCT-2P are synthesized in this work for the first time.

All four POFs are insoluble in common organic solvents such as THF, DMF, CH_2Cl_2 , acetone, and CHCl_3 , consistent to the expected highly crosslinked structure. Based on the scanning electron microscopy (SEM) images (Fig. S5 in ESI), except pTCT that exhibits a flaky morphology possibly due to its monomer's planar structure, the other POFs are composed of submicrometer particles and its aggregates. Thermal gravimetric analysis (TGA) reveals the good to excellent thermal stability of D-A POFs with significant thermal decomposition around 500 °C. (Fig. S6). Powder X-ray diffraction analysis suggests the amorphous nature of all POFs (Fig. S7). The presence of the absorption peak in FT-IR spectra at $\sim 805\text{ cm}^{-1}$ (assigned to the trisubstituted phenyl ring in carbazole polymer) also indicates the successful polymerization (Fig. S8).²⁴

The porosity parameters including Brunauer–Emmett–Teller (BET) (SA_{BET}) and pore volume of POFs were characterized by N_2 adsorption–desorption measurements at 77 K (Table 1 and Fig. S9 in ESI). A rapid N_2 uptake at low relative pressure ($P/P_0 < 0.05$) indicates the presence of typical micropores and the gradual increase of the N_2 uptake ($P/P_0 = 0.05 - 0.9$) is attributed to the presence of mesopores (i.e. pore width > 2 nm) in POFs. The coexistence micro- and mesopores and the pore network effect²⁵ are also manifested by the hysteresis between adsorption and desorption for all POFs (Fig. S9). The SA_{BET} of D-A POFs increases from pTCT-2P ($680\text{ m}^2\text{ g}^{-1}$), pTCT ($797\text{ m}^2\text{ g}^{-1}$), to pTCT-P

Table 1. SA_{BET} , Pore Volume, Photophysical Properties, and Redox Potentials of D-A POFs.

POFs	SA_{BET} ($\text{m}^2\text{ g}^{-1}$) ^a	V_{total} ($\text{cm}^3\text{ g}^{-1}$) ^b	V_{meso} ($\text{cm}^3\text{ g}^{-1}$) ^c	λ_{ex} (nm) ^d	λ_{em} (nm) ^d	$E_{1/2}^{\text{oxe}}$	$E_{1/2}^{\text{rede}}$	$*E_{1/2}^{\text{ox}}$	$*E_{1/2}^{\text{red}}$	E_{0-0}^f
pTCB	1404	0.76	0.40	343	460	+1.31			-1.81	3.12
pTCT	797	0.39	0.13	437 ^h	525		-1.04	+1.55		2.59
pTCT-P	1057	0.69	0.41	423 ^h	528	+1.48	-1.52	+1.12	-1.16	2.64
pTCT-2P	680	0.40	0.24	424 ^h	528	+1.45	-1.73	+0.91	-1.19	2.64

^aSurface area ($\text{m}^2\text{ g}^{-1}$) calculated from the nitrogen adsorption branch based on the BET model. ^bThe total pore volume ($\text{cm}^3\text{ g}^{-1}$) calculated at $P/P_0 = 0.95$. ^cThe volume of mesopores with pore width > 2 nm. ^dMeasured in polyethylene glycol 400. ^eAll potentials are given in volts versus the saturated calomel electrode (SCE). ^f E_{0-0} , the zero-zero vibrational state excitation energy, was estimated using the medium wavelengths between the photoluminescence excitation peak (λ_{ex}) and emission peak (λ_{em}) and was used to calculate $*E_{1/2}^{\text{ox}} (= E_{1/2}^{\text{red}} + E_{0-0})$ and $*E_{1/2}^{\text{red}} (= E_{0-0} - E_{1/2}^{\text{ox}})$. ^hThe shoulder peak at the longer wavelength was used.

(1057 m² g⁻¹) (Table 1), which agree well with the trend of solubility of the corresponding monomers in CHCl₃ (e.g. solubility: TCT-P > TCT > TCT-2P). Notably, despite the similar size of the corresponding monomer, pTCB has the highest SA_{BET} (1404 m² g⁻¹) and pore volume (0.76 cm³ g⁻¹), roughly two times larger than those of pTCT, which can also be explained by the excellent solubility of TCB in CHCl₃ that facilitates the smooth polymerization. Nevertheless, the presence of appreciably high percentage of mesoporous in all POFs (> 33%) indicates their suitability for the mass transport of substrates and products in the photocatalytic reactions (Fig. S10 in ESI).

As shown in Fig. 1b, pTCB, pTCT, pTCT-P, and pTCT-2P appear as light yellow, brown, yellow, and orange solid under visible light, and exhibit bright blue, red, bright yellow, and orange fluorescence under UV light irradiation ($\lambda_{\text{ex}} = 365 \text{ nm}$), respectively. They all exhibit broad absorption bands that extend to the visible region (Fig. S11 in ESI). Despite the color difference, the three D-A POFs have similar emission peaks around 525–528 nm, corresponding to comparable charge separation and recombination (Fig. S12). The excitation spectra, however, indicate that the intensity of charge transfer transition becomes weaker as the D-A distance becomes longer from pTCT to pTCT-2P (Fig. S12).

The free rotation of C–C and C–N single bonds in the carbazole-triazine D-A POFs results in the non-planarity and limited π -conjugation, thus they are best described as molecular photocatalysts. Cyclic voltammetry was then used to determine the ground state redox potentials of the POFs (Table 1 and Fig. S13 in ESI). The $E_{1/2}^{\text{ox}}$ of pTCB (+1.31 V vs SCE) is less positive than those of D-A POFs (+1.45 V and +1.48 V for pTCT-P and pTCT-2P, respectively); and as the D-A distance decreases, both $E_{1/2}^{\text{red}}$ and $*E_{1/2}^{\text{ox}}$ becomes more negative from pTCT (–1.04 V and +1.55 V, respectively) to pTCT-2P (–1.71 V and +0.91 V, respectively) due to their similar $E_{0,0'}$ values. Meanwhile, pTCB exhibits the most negative $*E_{1/2}^{\text{red}}$ value (–1.81 V), consistent with its electron donor nature. Overall, the incorporation of triazine increases the oxidative capability of D-A POFs, and as the D-A distance increases, the D-A POFs recover the reductive capability.

Photocatalytic activation of molecular oxygen

Reactive oxygen species (ROSs) such as superoxide radicals ($\text{O}_2^{\cdot-}$) and singlet oxygen ($^1\text{O}_2$) are important intermediates widely involved in oxidative organic transformations.²⁶ Our previous work has shown that carbazolic POFs (Cz-POFs) can efficiently generate $\text{O}_2^{\cdot-}$ through photoredox catalysis.¹⁶ Herein, we further test the potentials of the carbazole-triazine D-A POFs to generate $^1\text{O}_2$ via photosensitization (i.e. triplet-triplet energy transfer process).²⁷ Using TEMP (2,2,6,6-tetramethylpiperidine) as the trapping agent for $^1\text{O}_2$ and upon the exposure of visible light and oxygen, all three D-A POFs indeed exhibit the characteristic signal of TEMPO ((2,2,6,6-tetramethylpiperidin-1-yl)oxyl) (Fig. 2a). The strength of the EPR signal also indicates the photosensitization efficiency follows the order of pTCT >

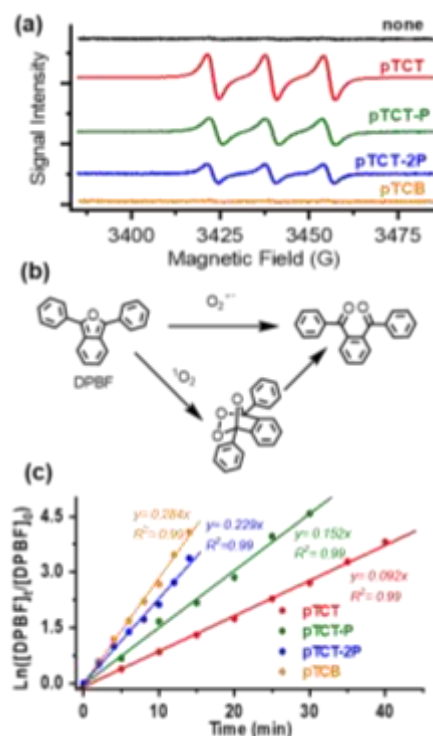


Fig. 2 (a) The EPR spectra of POFs in the presence of air and TEMP after visible light irradiation; (b) Photo-bleach reactions of DPBF; (c) The rate of DPBF bleaching promoted by different POFs.

pTCT-P > pTCT-2P under the same condition. No EPR signal is observed for pTCB, which indicates its poor efficiency of photogeneration of $^1\text{O}_2$.

We next use the photo-bleach experiment of 1,3-diphenylisobenzofuran (DPBF) to compare the overall efficiency of ROSs generation sensitized by all four POFs. It is known that DPBF can be oxidized by both $^1\text{O}_2$ and $\text{O}_2^{\cdot-}$ to the ketone compound (Fig. 2b), during which the absorption peak at 410 nm is bleached.²⁸ As shown in Fig. 2c and Fig. S14, DPBF bleaches faster in the presences of pTCB than the three D-A POFs. Because of its poor photosensitization capability for $^1\text{O}_2$, pTCB clearly is the most efficient catalyst to generate $\text{O}_2^{\cdot-}$. In addition, the overall ROSs generation efficiency increases in the order of pTCT-2P > pTCT-P > pTCT, opposite to the efficiency of $^1\text{O}_2$ generation. Therefore, it can be concluded that as the donor-acceptor distance increases in POFs, the efficiency of the D-A POFs to generate $^1\text{O}_2$ and $\text{O}_2^{\cdot-}$ decreases and increases, respectively.

Photocatalytic oxidation of sulfides

We first use selective sulfide oxidation as a model reaction to test the photocatalytic efficiency of the carbazole-triazine D-A POFs. Organic sulfoxides are important bioactive compounds in pharmaceutical chemistry and other chemical industries.²⁹ It is known that $^1\text{O}_2$ can selectively oxidize sulfides to sulfoxides with minimum over-oxidation.³⁰ With 0.5 mol% loading of pTCT, thioanisole was converted to methyl phenyl sulfoxide with high efficiency (95% yield, Table 2, entry 1) upon irradiation by a 26

Table 2. Optimization of Photocatalysts for the Aerobic Oxidation of Sulfides.^a

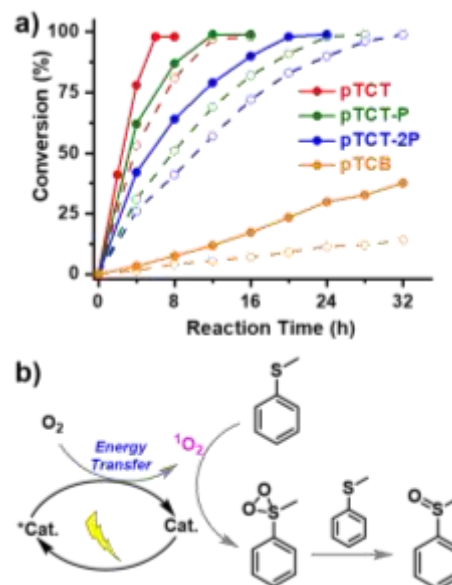
entry	photocatalyst	yield (%) ^b
1	pTCT	95 (12 h)
2	pTCT-P	94 (24 h)
3	pTCT-2P	93 (32 h)
4	pTCB	14 (32 h)
5	pTCT ^c	NR
6	pTCT ^d	94 (24 h)

^aStandard condition: 0.5 mol% photocatalyst, 0.4 mmol thioanisole, 5 mL MeOH, 26 W white CFL at room temperature. ^bIsolated yield. ^c2.0 equiv NaN₃. ^d2.0 equiv quinone.

W white compact fluorescent lamp (CPL) at room temperature for 12 h. Control experiments confirmed the essential role of photocatalyst, visible light, and air (Table S2, entries 2-4, ESI). The other two D-A POFs, pTCT-P and pTCT-2P, require longer reaction time (24 h and 32 h, respectively, Table 2, entries 2-3). Polymer pTCB exhibits a poor activity (14% yield in 32 h, Table 2, entry 4). These results are in line with the trend of ¹O₂ generation efficiency obtained from the EPR study (Fig. 2a). In the absence of the extended conjugation network, the corresponding monomers do not show any activity in this reaction (Table S2 in ESI, entries 5-8).

Several experiments further confirmed that the oxidation of sulfide to sulfoxide undergoes the ¹O₂ pathway. When 2.0 equiv of NaN₃ (¹O₂ quencher) was added into the reaction mixture, no product was detected (Table 2, entry 5). On the contrary, quinone, a well-known O₂^{•-} trapping agent, did not show any reaction inhibition (Table 2, entry 6). Moreover, the reaction was significantly accelerated for all POFs when the reaction was conducted in CD₃OD due to the longer lifetime of ¹O₂ in the deuterated solvent (Fig. 3a). Collectively, the sulfoxide formation indeed proceeds through the ¹O₂ oxidation pathway (Fig. 3b), which is in contrast with the O₂^{•-} mechanism proposed by Loh and coworkers.^{13d} Our result also suggests that ¹O₂ is more active than O₂^{•-} for the selective oxidation of sulfides. The high efficiency of D-A POFs for photosensitization may benefit from the stabilized charge separation triplet state. The doping of N atoms in triazine provides the *n*- π charge transfer and corresponding efficient intersystem crossing to afford the stabilized triplet excited state.

A wide scope of substrates was used to test the efficiency and selectivity of pTCT. As shown in Table 3, with 0.5 mol% loading, excellent yield and selectivity for both aryl sulfoxides and aliphatic sulfoxide were obtained. It is noted however that electron-withdrawing group such as chloro- and bromo- slightly decreases the reaction rate (Table 3, entries 4 and 5), consistent with previous reports.³¹ The aliphatic sulfide (**1F**) exhibits the highest reaction rate and selectivity (8 h, 98% yield, Table 3, reaction rate significantly decreases (48 h, 94% yield, Table 3,

**Fig. 3.** (a) Plots of conversion of thioanisole to methyl phenyl sulfoxide in CH₃OH (open circle) and CD₃OD (solid circle). (b) Proposed mechanism for the photocatalytic oxidation of thioanisole.

entry 8). It is also noted that as the sulfide size increases from **1A** to **1H**, the reaction rate of decreases about four times (Table 3, entries 1 and 8), likely due to the significantly larger size of **1H** that slows down its mass transport in the porous structure of the catalyst.

Table 3. Substrate Scope of the Aerobic Oxidation of Sulfides^a

entry	substrate	t (h)	conversion (%) ^b	selectivity ^{b,c}	yield ^d
1	1A	12	> 99	97 : 3	95
2	1B	16	> 99	95 : 5	94
3	1C	14	> 99	96 : 4	95
4	1D	18	> 99	98 : 2	97
5	1E	18	> 99	99 : 1	98
6	1F	8	> 99	99 : 1	98
7	1G	14	> 99	99 : 1	93
8 ^e	1H	48	> 99	95 : 5	94

^aReaction condition: 0.5 mol% pTCT, 0.4 mmol sulfide, 5 mL MeOH, 26 W white CPL at room temperature for 12 h. ^bConversion and selectivity were determined by ¹H NMR. ^cThe ratio between sulfoxide and sulfone. ^dIsolated yield. ^e0.2 mmol substrate was used.

Oxidative amine coupling

We next studied the photocatalytic performance of D-A POFs in the aerobic oxidation of primary amines to imines, a widely studied model reaction.³² In the presence of 0.5 mol% POFs, benzylamine was oxidized to the corresponding Schiff-base with excellent yield (Table 4). Again, control experiments confirmed the necessity of the photocatalyst, light irradiation, and air (Table S3, entries 2-4, ESI). The monomers exhibit significantly lower or no activity (Table S3, entry 5-8), highlighting that the polymerization indeed enhances the photocatalytic activities.

According to the previously proposed reaction mechanism, the oxidative amine coupling can undergo either an energy transfer ($^1\text{O}_2$) or electron transfer ($\text{O}_2^{\cdot-}$) pathway.³³ A comparative study shows that only pTCT exhibits a slightly improved reaction rate in the deuterated solvent (CD_3CN) (Fig. 4). Meanwhile, NaN_3 does not inhibit the reaction (Table 4, entry 5). Hence, most likely the reaction proceeds through the electron transfer ($\text{O}_2^{\cdot-}$) pathway (Fig. S17 in ESI) and the turnover of the photocatalyst requires two sequential single electron transfer (SET) steps, which generate benzylamine cation radical and $\text{O}_2^{\cdot-}$ that further react to each other to afford an electrophilic imine. The imine intermediate then attacks to another amine molecule to form the final product.

It is noted that D-A POFs have higher activity than pTCB (Table 4 and Fig. 4). For instance, pTCT-2P has highest efficiency (6 h, 98% yield, Table 4, entry 3) and the pTCB shows the lowest photocatalytic activity (24 h, 96% yield, Table 4, entry 4). Since pTCB has the fastest rate for ROSs generation, its low activity for this reaction is likely due to unfavored kinetics in the oxidation of benzylamine ($E_{1/2}^{\text{ox}} = +1.23 \text{ V}^{33}$). For the three D-A POFs, the photocatalytic activity slightly increases from pTCT to pTCT-2P, a trend consistent with the rate ROSs generation and subsequent O_2 reduction (Fig. 2c), which therefore indicates the amine oxidation is not rate limiting step.

The substrate scope was studied using pTCT-2P as the photocatalyst. Excellent conversion (> 99%) and selectivity (> 92%) were obtained for different derivatives benzylamine (Table 5). The substituent on the phenyl ring has an insignificant

Table 4. Screening Photocatalysts for the Oxidative Amine Coupling^a



entry	photocatalyst	yield (%) ^b
1	pTCT	97 (12 h)
2	pTCT-P	98 (8 h)
3	pTCT-2P	98 (6 h)
4	pTCB	96 (24 h)
5	pTCT	96 (12 h) ^c

^aStandard condition: 0.5 mol% photocatalyst, 0.4 mmol benzylamine, 5 mL MeCN, 26 W white CFL at room temperature. ^bDetermined by ^1H NMR. ^c2.0 equiv NaN_3 .

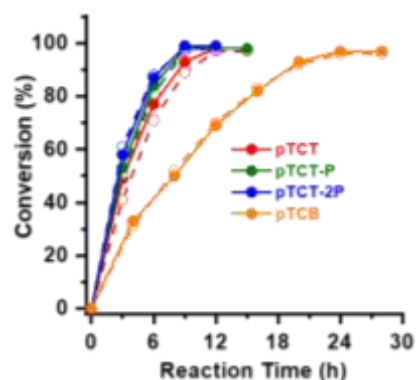


Fig. 4. Photocatalytic benzylamine coupling in CH_3CN (open circle) and CD_3CN (solid circle).

effect on the reaction rate and selectivity. In general, electron withdrawing group accelerates (Table 5, entries 2-3) and electron donating group decelerates the reaction (Table 5, entries 4-5). In the cases of heterocyclic methylamines, a longer reaction time is needed (e.g. pyridin-4-yl-, furan-2-yl-, and thiophen-2-yl-, Table 5, entries 6-8), consistent with previous results where TiO_2 was used as the photocatalyst.³⁴ With the high yield and excellent selectivity, the obtained Schiff-bases can be easily applied for further organic synthesis. For example, after the photocatalytic amine coupling, an Ugi-type reaction can be directly conducted without purification (Fig. S4 in ESI).³⁵ For both the electron donating and withdrawing substrates, the di-amide products, which can be transferred to α -amino acid, were obtained with good isolated yields (76%–86%).

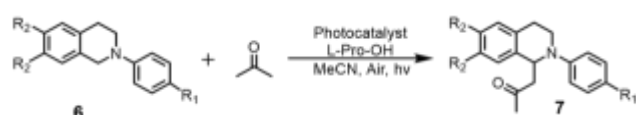
Aerobic photo-oxidative Mannich reaction

The potential application of POFs in the well-studied photo-oxidative Mannich reaction was also studied.³⁶ This

Table 5. Substrate Scope of the Photocatalytic Oxidative Amine Coupling^a

entry	substrate	t (h)	conversion ^b	selectivity ^{b,c}
1	3A	8	> 99%	98 : 1
2	3B	4	> 99%	99 : 1
3	3C	5	> 99%	99 : 1
4	3D	10	> 99%	96 : 1
5	3E	12	> 99%	98 : 1
6	3F	36	> 99%	92 : 8
7	3G	24	> 99%	99 : 1
8	3H	30	> 99%	99 : 1

^aReaction condition: 0.5 mol% pTCT-2P, 0.4 mmol thioether, 5 mL MeOH, 26 W white light at room temperature. ^bConversion and selectivity was tested by ^1H NMR. ^cThe byproduct is the corresponding aryl aldehyde.

Table 6. Aerobic Photo-oxidative Mannich Reaction.^a

entry	substrate	R ₁ , R ₂	yield (%) ^b
1	6A	R ₁ = H, R ₂ = H	96 (18 h) ^c
2	6A	R ₁ = H, R ₂ = H	98 (6 h)
3	6A	R ₁ = H, R ₂ = H	95 (8 h) ^d
4	6A	R ₁ = H, R ₂ = H	96 (10 h) ^e
5	6B	R ₁ = H, R ₂ = Br	96 (6 h)
6	6C	R ₁ = H, R ₂ = OMe	96 (6 h)
7	6D	R ₁ = OMe, R ₂ = H	96 (6 h)
8	6E	R ₁ = OMe, R ₂ = Br	90 (6 h)
9	6F	R ₁ = OMe, R ₂ = OMe	86 (24 h)
10	6G	R ₁ = tBu, R ₂ = H	98% (6 h)

^aStandard condition: 0.5 mol% pTCT-P, 0.25 mmol substrate, 2.5 mmol acetone, 0.05 mmol L-Proline, 5 mL MeCN, 26 W white CPL at room temperature for 6 h. ^bIsolated yield. ^cpTCT as catalyst. ^dpTCT-2P as catalyst. ^epTCB as catalyst.

C(sp³)-C(sp³) cross-coupling reaction involves the oxidative activation of the α -amino C-H bond to generate reactive iminium ions and subsequent C-C bond formation between the iminium ions and a nucleophilic imine (Fig. S19 in ESI). With 0.5 mol% loading of POFs as the photocatalyst, an excellent yield (95%–98%) was achieved after visible light irradiation of an aerated mixture containing *N*-phenyl-tetrahydroisoquinoline (**3A**) and L-proline (co-catalyst) in the presence of acetone (Fig. S18). Different from the amine coupling reaction, pTCT-P exhibits the highest catalytic activity (6 h, 98%, Table 6, entry 2), which is better than both highly reductive pTCB (10 h, 96%, Table 6, entry 4) and highly oxidative pTCT (18 h, 96%, Table 6, entry 1). This result suggests that a balanced O₂ reduction and amine oxidation is critical to this reaction and highlights the necessity of modulating the photoredox properties of POFs for catalytic applications.

A wide scope of substrates was used to test the effect of substituent on the reaction. As shown in Table 6, with 0.5 mol% pTCT-P as the photocatalyst, the cross-dehydrogenative coupling products with acetone were obtained in good to

excellent yields (86%–98%). Both the electron donating group (-OMe) and electron withdrawing group (-Br) on the *N*-phenyl or tetrahydroisoquinoline did not affect the reaction rate (Table 6, entries 6-8). However, for the substrate **6F** where both *N*-phenyl and tetrahydroisoquinoline contain a methoxyl group, both the reaction rate and yield decreased (Table 6, entry 9).

Recyclability and stability

Recyclability of the POFs were tested for all three reactions. As for the sulfides oxidation, the conversion can still reach 95% and 96% for pTCT-P and pTCT-2P after five times of reuse, respectively (Fig. 6a). However, a noticeable decrease of conversion from 99% to 68% was found for pTCT. A similar trend was observed in the oxidative amine coupling and Mannich reactions. The pTCT-P, pTCT-2P, and pTCB show excellent recyclability: after five times of reuse, the decay of reaction conversion is less than 5% (Fig. 6b-c). When pTCT was used for these two reactions, however, the decay of conversion was faster, specifically, decreased from 95% to 71% for amine coupling (Fig. 6b) and from 97% to 67% for Mannich reaction (Fig. 6c), respectively. The chemical stability of the POFs was investigated by FT-IR spectroscopy. The recovered pTCT-P, pTCT-2P, and pTCB did not show significant change compared with the original sample, indicating their high stability. However, a new peak at 1736 cm⁻¹ corresponding to C=O bond appears in the FT-IR spectra of the recovered pTCT, which indicates the partly oxidation of pTCT during the reaction (Fig. S20 in ESI).

Conclusions

In summary, we reported the preparation of carbazole-triazine based D-A POFs and their applications in three prototypic photocatalytic aerobic oxidation reactions. The incorporation of the triazine-based electron acceptor into D-A POFs induces an efficient photoinduced charge separation, which promotes the triplet-triplet energy transfer pathway to generate ¹O₂. Meanwhile, the redox potentials in both ground state and excited state can be controlled via the adjustment of the D-A distance in the monomer. Correspondingly, the photocatalytic activities of D-A can be fine-tuned. Sulfides oxidation, oxidative

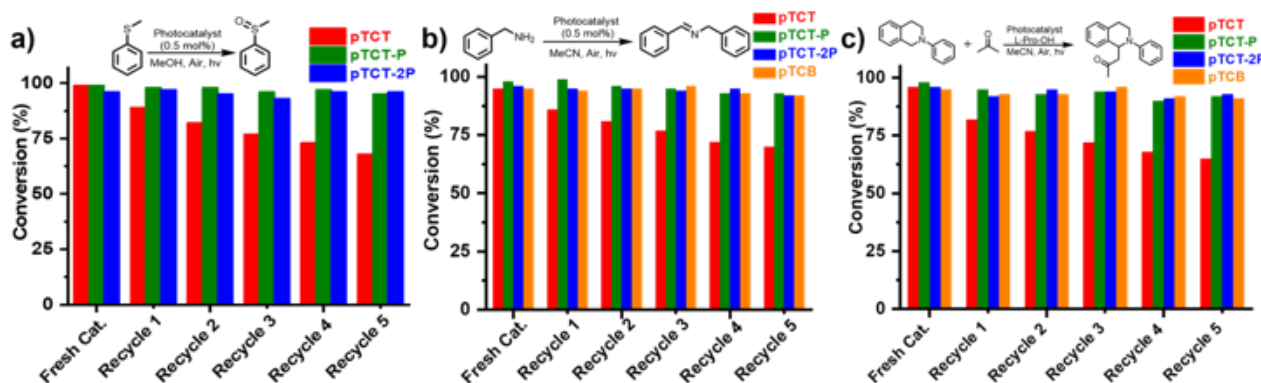


Fig. 6. Recyclability of POFs in (a) sulfide oxidation; (b) amine coupling; and (c) Mannich reaction. Reaction time was fixed for each cycle.

amine coupling, and Mannich reaction were chosen to investigate the catalytic activity of the POFs. Due to their outstanding capability to generate the ROSs and tunable redox potentials, the D-A POFs shown significant higher photocatalytic activity in all these three reactions than pTCB that is only composed of carbazole donor. This work provides a guidance for the future design of the porous metal-free photocatalysts with broad substrate scope.

Conflicts of interest

There are no conflicts to declare.

Acknowledgements

J.Z. acknowledges a National Science Foundation CAREER Award (DMR-1554918) for support of this research.

References

- (a) A. M. Thayer, *Chem. Eng. News*, 1992, **70**, 27; (b) Z. Guo, B. Liu, Q. Zhang, W. Deng, Y. Wang and Y. Yang, *Chem. Soc. Rev.*, 2014, **43**, 3480.
- (a) H. Tohma and Y. Kita, *Adv. Synth. Catal.*, 2004, **346**, 111; (b) T. Punniyamurthy, S. Velusamy and J. Iqbal, *Chem. Rev.*, 2005, **105**, 2329.
- (a) B.-Z. Zhan and A. Thompson, *Tetrahedron*, 2004, **60**, 2917; (b) T. Mallat and A. Baiker, *Chem. Rev.*, 2004, **104**, 3037; (c) K. Kaneda, K. Ebitani, T. Mizugaki and K. Mori, *Bull. Chem. Soc. Jpn.*, 2006, **79**, 981; (d) T. Matsumoto, M. Ueno, N. Wang and S. Kobayashi, *Chem.-Asian J.*, 2008, **3**, 196.
- (a) M. Pagliaro, S. Campestrini and R. Ciriminna, *Chem. Soc. Rev.*, 2005, **34**, 837; (b) T. Suzuki, *Chem. Rev.*, 2011, **111**, 1825; (c) Z. Shi, C. Zhang, C. Tang and N. Jiao, *Chem. Soc. Rev.*, 2012, **41**, 3381; (d) M. Stratakis and H. Garcia, *Chem. Rev.*, 2012, **112**, 4469; (e) S. E. Allen, R. R. Walvoord, R. Padilla-Salinas and M. C. Kozlowski, *Chem. Rev.*, 2013, **113**, 6234.
- (a) M. A. Ischay, M. E. Anzovino, J. Du and T. P. Yoon, *J. Am. Chem. Soc.*, 2008, **130**, 12886; (b) D. A. Nicewicz and D. W. C. MacMillan, *Science*, 2008, **322**, 77; (c) J. M. Narayanam, J. W. Tucker and C. R. Stephenson, *J. Am. Chem. Soc.*, 2009, **131**, 8756; (d) C. K. Prier, D. A. Rankic and D. W. MacMillan, *Chem. Rev.*, 2013, **113**, 5322.
- (a) J. M. Narayanam and C. R. Stephenson, *Chem. Soc. Rev.*, 2011, **40**, 102; (b) I. Ghosh, T. Ghosh, J. I. Bardagi and B. König, *Science*, 2014, **346**, 725; (c) J. C. Theriot, C. H. Lim, H. Yang, M. D. Ryan, C. B. Musgrave and G. M. Miyake, *Science*, 2016, **352**, 1082; (d) S. P. Pitre, C. D. McTiernan and J. C. Scaiano, *Acc. Chem. Res.*, 2016, **49**, 1320; (e) M. Majek and A. Jacobi von Wangelin, *Acc. Chem. Res.*, 2016, **49**, 2316; (f) D. M. Arias-Rotondo and J. K. McCusker, *Chem. Soc. Rev.*, 2016, **45**, 5803; (g) N. A. Romero and D. A. Nicewicz, *Chem. Rev.*, 2016, **116**, 10075.
- X. Lang, X. Chen and J. Zhao, *Chem. Soc. Rev.*, 2014, **43**, 473.
- X. Wang, K. Maeda, A. Thomas, K. Takanebe, G. Xin, J. M. Carlsson, K. Domen and M. Antonietti, *Nat. Mater.*, 2009, **8**, 76.
- R. Li, Z. J. Wang, L. Wang, B. C. Ma, S. Ghasimi, H. Lu, K. Landfester and K. A. I. Zhang, *ACS Catal.*, 2016, 1113.
- (a) K. Zhang, D. Kopetzki, P. H. Seeberger, M. Antonietti and F. Vilela, *Angew. Chem., Int. Ed.*, 2013, **52**, 1432; (b) Y. L. Wong, J. M. Tobin, Z. Xu and F. Vilela, *J. Mater. Chem. A*, 2016, **4**, 18677.
- (a) J. X. Jiang, F. Su, A. Trewin, C. D. Wood, N. L. Campbell, H. Niu, C. Dickinson, A. Y. Ganin, M. J. Rosseinsky, Y. Z. Khimyak and A. I. Cooper, *Angew. Chem., Int. Ed.*, 2007, **46**, 8574; (b) P. Kaur, J. T. Hupp and S. T. Nguyen, *ACS Catal.*, 2011, **1**, 819; (c) D. Wu, F. Xu, B. Sun, R. Fu, H. He and K. Matyjaszewski, *Chem. Rev.*, 2012, **112**, 3959; (d) Y. Zhu, H. Yang, Y. Jin and W. Zhang, *Chem. Mater.*, 2013, **25**, 3718; (e) X. Zou, H. Ren and G. Zhu, *Chem. Commun.*, 2013, **49**, 3925; (f) S. Das, P. Heasman, T. Ben and S. Qiu, *Chem. Rev.*, 2017, **117**, 1515; (g) W. Huang, B. C. Ma, H. Lu, R. Li, L. Wang, K. Landfester and K. A. I. Zhang, *ACS Catal.*, 2017, 5438; (h) C. B. Meier, R. S. Sprick, A. Monti, P. Guigliion, J.-S. M. Lee, M. A. Zwijnenburg and A. I. Cooper, *Polymer*, 2017, **126**, 283; (i) J. Bi, W. Fang, L. Li, J. Wang, S. Liang, Y. He, M. Liu and L. Wu, *Macromol. Rapid Commun.*, 2015, **36**, 1799.
- (a) Z. Xie, C. Wang, K. E. deKrafft and W. Lin, *J. Am. Chem. Soc.*, 2011, **133**, 2056; (b) J.-L. Wang, C. Wang, K. E. deKrafft and W. Lin, *ACS Catal.*, 2012, **2**, 417; (c) H.-P. Liang, Q. Chen and B.-H. Han, *ACS Catal.*, 2018, 5313; (d) Q. Chen, J.-X. Wang, F. Yang, D. Zhou, N. Bian, X.-J. Zhang, C.-G. Yan and B.-H. Han, *J. Mater. Chem.*, 2011, **21**, 13554; (e) J.-H. Zhu, Q. Chen, Z.-Y. Sui, L. Pan, J. Yu and B.-H. Han, *J. Mater. Chem. A*, 2014, **2**, 16181.
- (a) Z. J. Wang, S. Ghasimi, K. Landfester and K. A. Zhang, *Chem. Commun.*, 2014, **50**, 8177; (b) Z. J. Wang, S. Ghasimi, K. Landfester and K. A. Zhang, *Adv. Mater. (Weinheim, Ger.)*, 2015, **27**, 6265; (c) M. Liras, M. Iglesias and F. Sánchez, *Macromolecules*, 2016, **49**, 1666; (d) C. Su, R. Tandiana, B. Tian, A. Sengupta, W. Tang, J. Su and K. P. Loh, *ACS Catal.*, 2016, 3594.
- Z. J. Wang, S. Ghasimi, K. Landfester and K. A. I. Zhang, *J. Mater. Chem. A*, 2014, **2**, 18720.
- (a) S. Dadashi-Silab, H. Bildirir, R. Dawson, A. Thomas and Y. Yagci, *Macromolecules*, 2014, **47**, 4607; (b) Z. J. Wang, S. Ghasimi, K. Landfester and K. A. I. Zhang, *Adv. Synth. Catal.*, 2016, **358**, 2576.
- J. Luo, X. Zhang and J. Zhang, *ACS Catal.*, 2015, **5**, 2250.
- Z. J. Wang, K. Garth, S. Ghasimi, K. Landfester and K. A. Zhang, *ChemSusChem*, 2015, **8**, 3459.
- J. Luo, X. Zhang, J. Lu and J. Zhang, *ACS Catal.*, 2017, **7**, 5062.
- (a) P. Kuhn, M. Antonietti and A. Thomas, *Angew. Chem., Int. Ed.*, 2008, **47**, 3450; (b) W. Huang, Z. J. Wang, B. C. Ma, S. Ghasimi, D. Gehrig, F. Laquai, K. Landfester and K. A. I. Zhang, *J. Mater. Chem. A*, 2016, **4**, 7555.
- (a) X. Zhang, J. Z. Lu and J. Zhang, *Chem. Mater.*, 2014, **26**, 4023; (b) Y. Zhang, S. A. Y. Zou, X. Luo, Z. Li, H. Xia, X. Liu and Y. Mu, *J. Mater. Chem. A*, 2014, **2**, 13422.
- Q. Chen, D. P. Liu, M. Luo, L. J. Feng, Y. C. Zhao and B. H. Han, *Small*, 2014, **10**, 308.
- Q. Chen, M. Luo, P. Hammershøj, D. Zhou, Y. Han, B. W. Laursen, C. G. Yan and B. H. Han, *J. Am. Chem. Soc.*, 2012, **134**, 6084.
- (a) H. Wang, Z. Cheng, Y. Liao, J. Li, J. Weber, A. Thomas and C. F. J. Faul, *Chem. Mater.*, 2017, **29**, 4885; (b) M. Saleh, S. B. Baek, H. M. Lee and K. S. Kim, *J. Phys. Chem. C*, 2015, **119**, 5395.
- C. Gu, N. Huang, J. Gao, F. Xu, Y. Xu and D. Jiang, *Angew. Chem., Int. Ed.*, 2014, **53**, 4850.
- P. M. Budd, E. S. Elabas, B. S. Ghanem, S. Makhseed, N. B. McKeown, K. J. Msayib, C. E. Tattershall and D. Wang, *Adv. Mater. (Weinheim, Ger.)*, 2004, **16**, 456.
- (a) H. H. Wasserman and J. L. Ives, *Tetrahedron*, 1981, **37**, 1825; (b) Y. Moro-oka, *Catal. Today*, 1998, **45**, 3; (c) M. Hayyan, M. A. Hashim and I. M. AlNashef, *Chem. Rev.*, 2016, **116**, 3029.

27. (a) J. Zhao, W. Wu, J. Sun and S. Guo, *Chem. Soc. Rev.*, 2013, **42**, 5323; (b) Z. Zhou, J. Song, L. Nie and X. Chen, *Chem. Soc. Rev.*, 2016, **45**, 6597.
28. A. Gomes, E. Fernandes and J. L. Lima, *J. Biochem. Biophys. Methods*, 2005, **65**, 45.
29. (a) D. A. Evans, M. M. Faul, L. Colombo, J. J. Bisaha, J. Clardy and D. Cherry, *J. Am. Chem. Soc.*, 1992, **114**, 5977; (b) I. Fernandez and N. Khair, *Chem. Rev.*, 2003, **103**, 3651; (c) J. Legros, J. R. Dehli and C. Bolm, *Adv. Synth. Catal.*, 2005, **347**, 19.
30. (a) F. Jensen, A. Greer and E. L. Clennan, *J. Am. Chem. Soc.*, 1998, **120**, 4439; (b) E. L. Clennan and A. Pace, *Tetrahedron*, 2005, **61**, 6665.
31. (a) J. Dad'ová, E. Svobodová, M. Sikorski, B. König and R. Cibulka, *ChemCatChem*, 2012, **4**, 620; (b) J. A. Johnson, X. Zhang, T. C. Reeson, Y. S. Chen and J. Zhang, *J. Am. Chem. Soc.*, 2014, **136**, 15881.
32. (a) F. Su, S. C. Mathew, L. Möhlmann, M. Antonietti, X. Wang and S. Blechert, *Angew. Chem., Int. Ed.*, 2011, **50**, 657; (b) M. Rueping, C. Vila, A. Szadkowska, R. M. Koenigs and J. Fronert, *ACS Catal.*, 2012, **2**, 2810.
33. J. A. Johnson, J. Luo, X. Zhang, Y. S. Chen, M. D. Morton, E. Echeverria, F. E. Torres and J. Zhang, *ACS Catal.*, 2015, **5**, 5283.
34. X. Lang, H. Ji, C. Chen, W. Ma and J. Zhao, *Angew. Chem., Int. Ed.*, 2011, **50**, 3934.
35. G. Jiang, J. Chen, J. S. Huang and C. M. Che, *Org. Lett.*, 2009, **11**, 4568.
36. M. Rueping, C. Vila, R. M. Koenigs, K. Poscharyny and D. C. Fabry, *Chem. Commun.*, 2011, **47**, 2360.

Table of Contents Entry

Carbazole-triazine based donor-acceptor porous organic frameworks are efficient photocatalysts for aerobic oxidation reactions.

